THE USE OF SERRATED LEADING EDGE FOR INFLOW CONDITIONING IN CENTRIFUGAL FAN

Lucio CARDILLO [3], Alessandro CORSINI [2,3], Giovanni DELIBRA [2], Anthony Geoffrey SHEARD [1], Lorenzo TIEGHI [2]

[1] *AGS Consulting Llc, Atlanta, USA*

[2] *Dipartimento di Ingegneria Meccanica e Aerospaziale, Sapienza Università di Roma, Rome, Italy*

[3] *SED Soluzioni per Energia e Diagnostica Srl, Ferentino, Italy*

SUMMARY

Fans are used as ancillaries units in many different applications, and usually designed in series and therefore need to deal with the fact that once installed can be requested to operate in non-optimal conditions. For designers and manufacturers this is a problem, as they are requested to design and build robust fans, able to operate in presence of strong inflow distortions or in complex and compact ventilation systems. Therefore it is important to have solutions that allow fans to perform, without being driven into unstable operations, even if installed improperly.

Here we present a numerical study to investigate the possibility of using serrated leading edges to minimize the effects of distorted inflow conditions in centrifugal fans. In particular a roof fan unit was chosen and sinusoidal leading edges applied to the impeller.

Numerical computations were performed with OpenFOAM with the cubic k-ε model of Lien and Leschziner on the datum fan.

In the final paper a comparison of performance with respect to the datum fan will be presented, highlighting how the modified leading edge impacts the fluid dynamics of the impeller and its performance in clean conditions and with the distorted inflow.

INTRODUCTION

Fans are industrial turbomachinery that derive most of the aerodynamic design techniques from aerospace industry, in particular from compressors. However, the peculiarity of fans is related to their use as industrial ancillaries, often as low-cost devices, that requires them to work in off-design conditions or / and in ventilation systems with arrangement that result in complex and unforeseen

inflow conditions. Moreover, the need for manufacturers to cut production costs, often results in design constraints that further limit the use of technical solutions that allow fans to work with reasonable performance in a wide range of operations (e.g. variable pitch in motion, high three-dimensionality of blade profiles) [1]. In the following we focus on a centrifugal fan for roof unit, characterized by two identical parallel disks connected with 9 non-twisted blades with constant cross-section and straight leading and trailing edges. The impeller discharge has no volute. Due to the lack of twist and tapering of the leading edge, the fan has a non-optimal alignment of the rotor with the incoming flow and this results in leading edge separation near the impeller disk, that becomes stronger when the fan is operating off-design or with dirty inflow conditions. We are now focusing on the possibility of using a wavy leading edge to reduce these problems, following the findings of [1] of the capability of such profiles to control separation and stall of the blade sections and therefore to extend the operating range of the fan.

ROOF FAN

The roof fan unit we focus on, Figure 1, has an impeller with two identical parallel disks used as shroud and back-shroud, connected by 9 blades extruded normally from a NACA profile in a backward arrangement. At the inlet a bellmouth is present. The impeller discharges directly into open air, without a volute. Design flow rate is 0.26 m^3/s with a rotational speed of 2000 rpm. Major features of the fan unit are summarized in

Table 1.

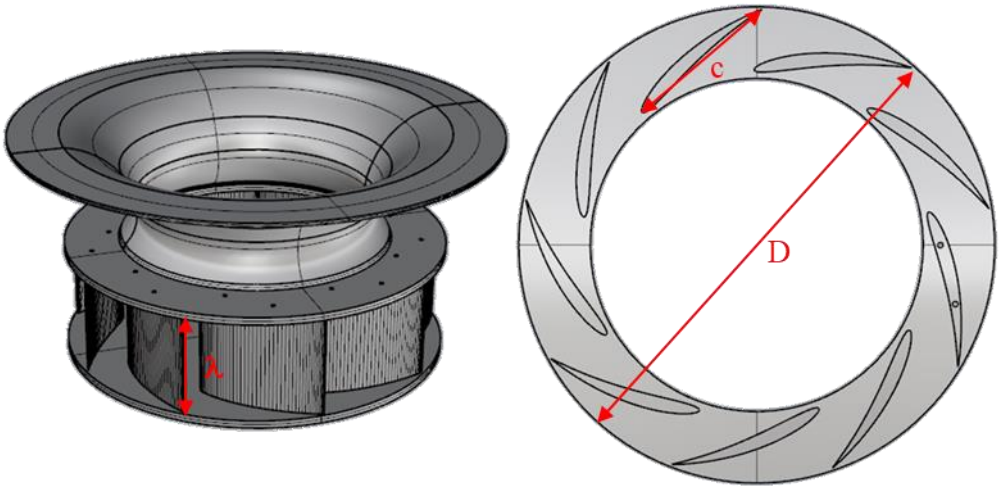

Figure 1 – 3D view of roof fan unit (left) and top view of the disk of the impeller with blades (right)

Table 1 – Summary of roof fan unit features

Maximum impeller diameter	D	254 mm
Design flow rate	Q_{DES}	0.26 m^3/s
Rotational speed	ω	2000 rpm
Blade aspect ratio (span/chord)	λ/c	0.79
Blade count	Z	9

NUMERICAL METHOD

Solvers and numerical schemes

Computations were carried out with the C^{++} open-source code OpenFOAM 2.3.x using the *SRFSimpleFoam* solver for steady-state computations of incompressible flows in the relative frame of reference. The Generalized Algebraic Multi-Grid solver was used for pressure, while all the other equations were solved with a Gauss–Seidel solver. Convergence threshold was set to 10^{-7} for pressure and to 10^{-5} for the other quantities. Turbulence modelling relied on the low-Reynolds cubic model of [2] that allows for a partial reproduction of anisotropy of Reynolds stresses.

Grid details, computational domain

The computational domain, Figure 2, entails one blade-to-blade passage, with periodic boundary conditions imposed at mid-pitch. The inflow entails a sector of a sphere with a diameter equal to 3.5 diameters at the bellmouth, while the outflow extends 1.5D down-stream of the blade trailing edge, corresponding to the outflow of the fan. Grid independence of the results was assessed using static pressure rise and torque as convergence parameters. Convergence of parameters was reached with a final computational grid that entails 4M hexahedra clustered along the hub, casing and the blade profile, Figure 3, for the datum impeller. For the modified impeller it was necessary to increase the number of cells in the axial direction to follow the sinusoidal leading edge without compromising with the quality of the mesh, and convergence of results was achieved with 8M hexahedra, Figure 4. Mesh quality indicators are summarized in Table 2 for both geometries.

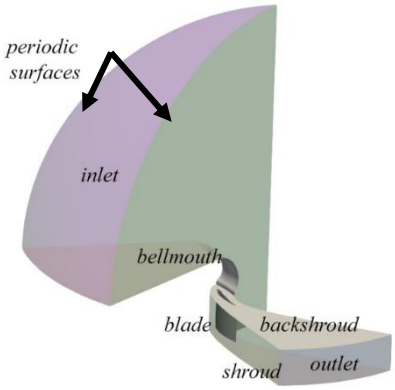

Figure 2 – Computational domain

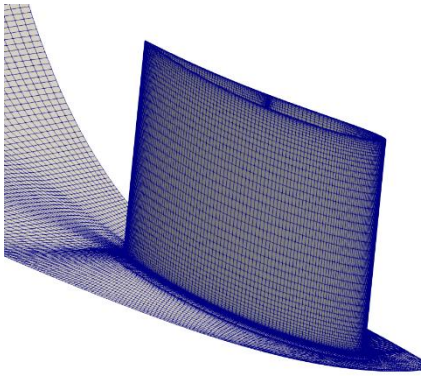

Figure 3 – Detail of the mesh at the junction between blade and shroud for the datum impeller

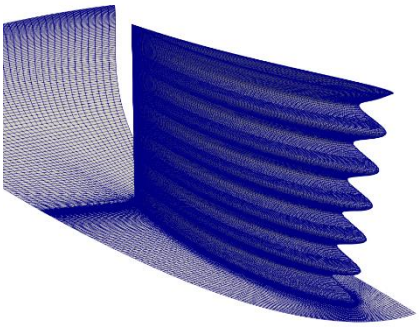

Figure 4 – Detail of the mesh at the junction between blade and shroud for the modified impeller

Table 2 - Mesh quality and y+ values

	datum impeller			***modified impeller***		
	Minimum	Maximum	Average	Minimum	Maximum	Average
Volume ratio	1	10	1.2	1	11	1.3
Aspect ratio	1	120	8	1	108	5.2
Skewness	0	0.6	0.08	0	0.66	0.09
Min. included angle	20	90	71	18	90	73
y^+	0.1	3.32	1.9	0.1	3.5	1.8

Boundary conditions

The inflow mass flow was specified, with a level of turbulence equal to 5%. At the outlet of the domain convective boundary conditions were specified. Over the inflow bellmouth surface absolute velocity was imposed equal to zero, while for the blade and the hub velocity was imposed coherently with the full speed of the fan. We set k and ε to zero over all the solid walls following a well-known redefinition of the ε equation.

RESULTS

Validation

Validation of numerical computations was carried out against available measured data, in terms of static pressure rise and mechanical power, Table 3. Discrepancy of pressure rise capability is within the limits of AMCA 210 [3] while error in power is below the tolerance of measurements, confirming that the setup was correctly reproduced.

Table 3 – Comparison of measured and computed pressure rise and power

	Δp_{stat}	power
exp	212 Pa	70.0 W
CFD	203 Pa	69.6 W
Δ	4 %	-

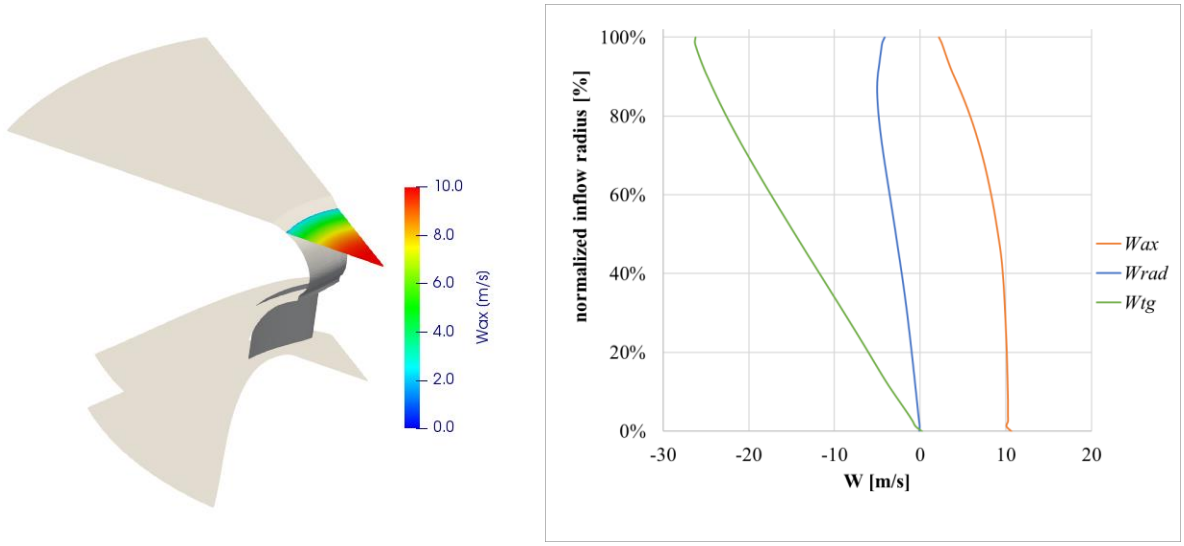

Figure 5 – Relative velocity components at the fan inflow, see insert on the left

Flow survey

When the fan is working with a clean inflow, the velocity profiles at the bellmouth, Figure 5, the only distortion is that due to the bellmouth itself, with a reduction of axial component near the bellmouth and the presence of a radial component due to the restriction of the inflow section.

As mentioned above, manufacture constraints does not allow for a twisted nor a tapered leading edge, as blade sections need to have a normal-to-the-disks staking line. This results, Figure 6, in the upper sections of the blade, near the shroud, to be characterized by separation on the second half of the suction surface. This separation interacts with the following blade, constraining the flow in the first 1/3 of the pressure surface near the leading edge, leading to loss of efficiency. Moving towards midspan towards the shroud, the flow results to be well-aligned with the leading edge of the impeller blade.

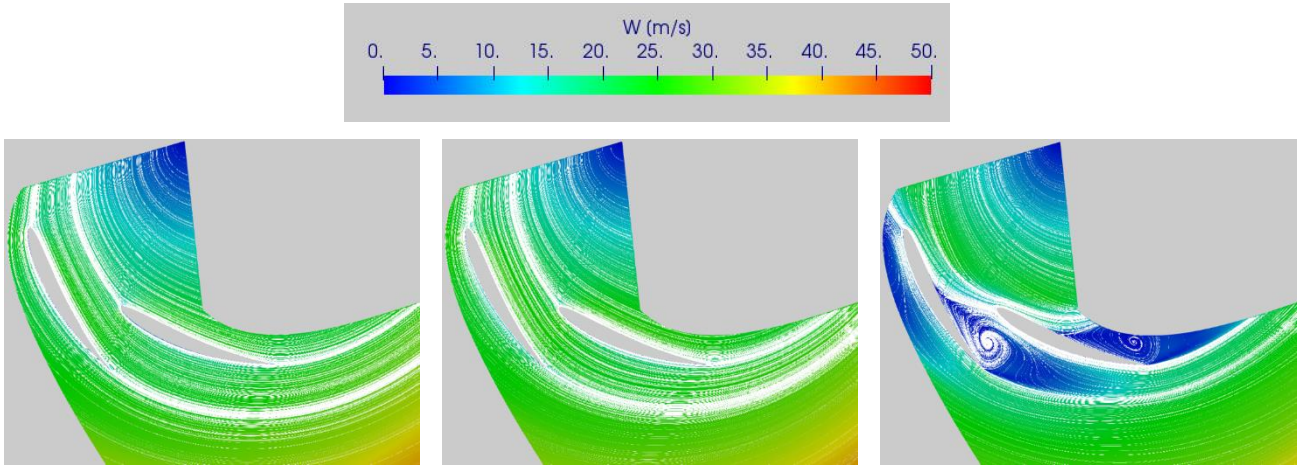

Figure 6 – Datum impeller: relative velocity streamlines over relative velocity contours for axial cross-sections at 10% (shroud), 50% and 90% (back-shroud) of the blade span

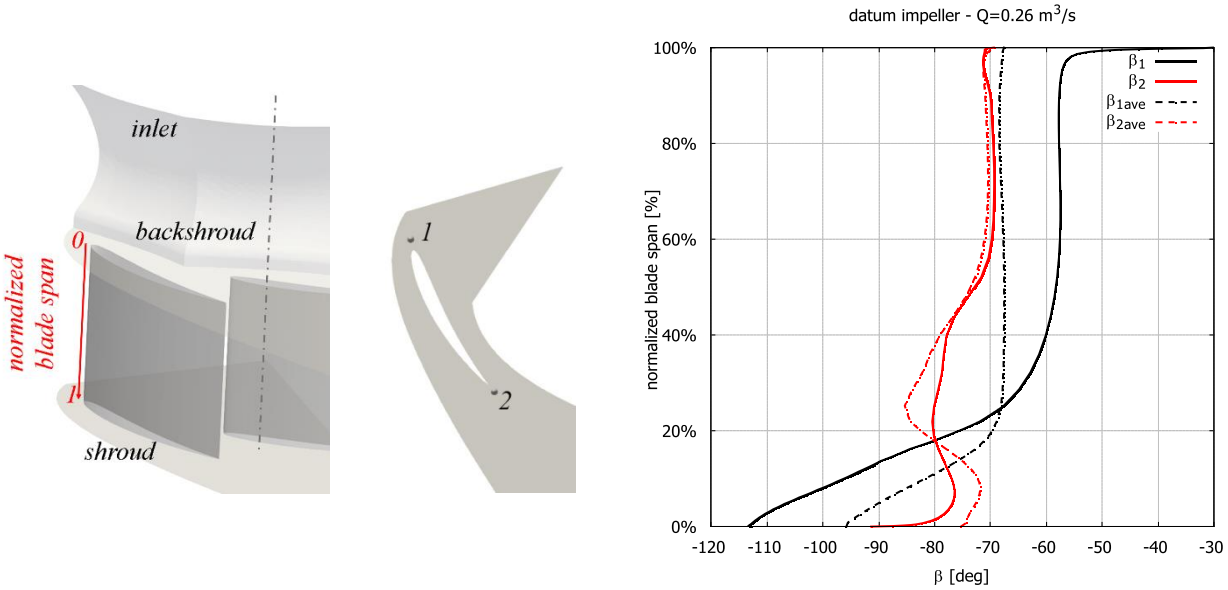

Figure 7 – Datum impeller: β_1 and β_2 spanwise distributions near the leading and trailing edges (see insert) and blade-to-blade averaged distributions (dashed lines)

From distribution of β_1 and β_2 spanwise distributions, Figure 7, the effect of the backshroud separation is evident, with a strong reduction of β_1 for the lower 40% of the blade span near the leading edge of the blade. In view of design of the blade, we can focus on the blade-to-blade averaged values of β_1 (dashed lines) and this effect results mitigated to the lower 20 % of the span of the blade.

The separation near the backshroud also results in an increase of axial velocity in the lower portion of the blade, Figure 8, and a strong reduction of radial velocity in the inflow section, Figure 8. The flow distortion is evident in this region with the comparison of the leading edge profiles and the blade-to-blade averaged profiles. However what is also evident is that this effect has a strong results in terms of exit velocity distribution, as the blade is not able to re-accommodate the flow axially and therefore strong velocity defect are still present.

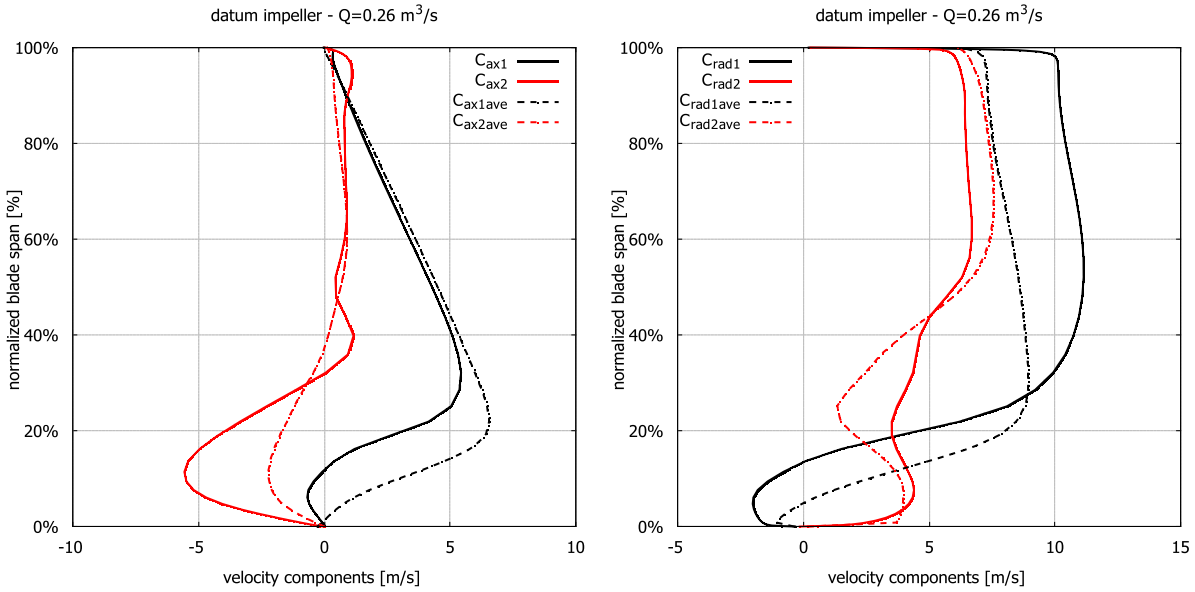

Figure 8 – Datum impeller: axial (left) and radial (right) velocity components spanwise distributions near the leading and trailing edges and blade-to-blade averaged distributions (dashed lines)

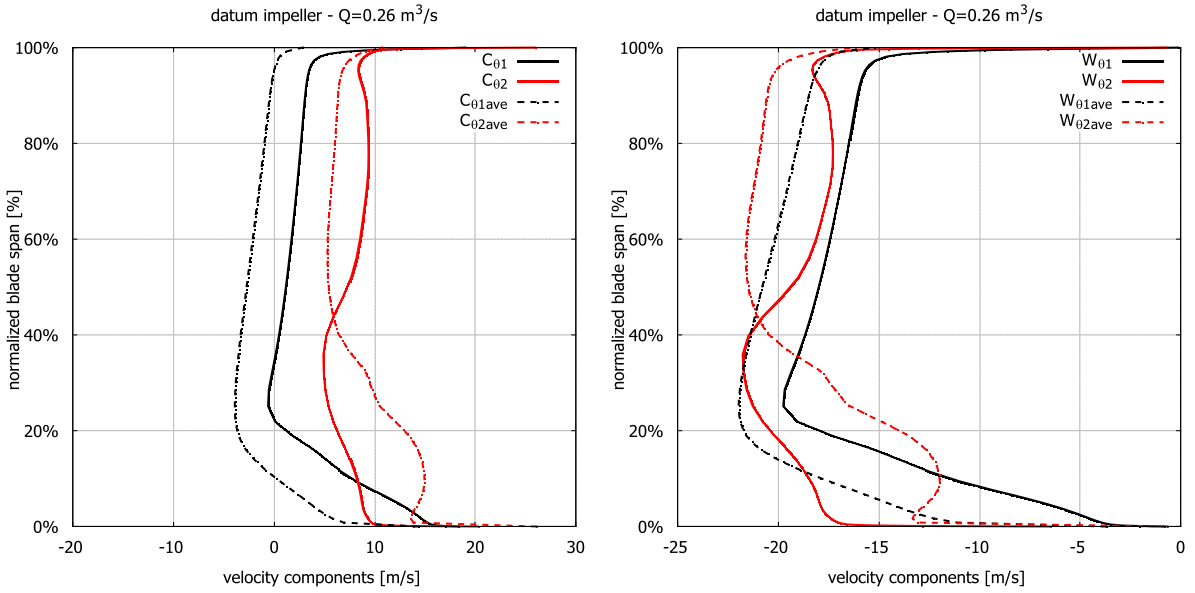

Figure 9 - Datum impeller: absolute (left) and relative (right) velocity components spanwise distributions near the leading and trailing edges and blade-to-blade averaged distributions (dashed lines)

If we focus on tangential velocity components, Figure 9, the effect is even more evident at the outflow section from plots of the relative tangential velocity, that show a sudden drop in the lower 20 % of the blade due to the aforementioned distortion.

Design of wavy leading edge

We designed a sinusoidal leading edge, [1] , to control trailing edge separation. In particular, this was based on the idea that can such modification can help redistributing the flow in the axial direction. To this aim the velocity profiles in Figure 8 and Figure 9 where analyzed to measure the average and maximum velocity defects along the blade. In this way it was possible to design a sinusoid able to close trailing edge separations, [1], Figure 10.

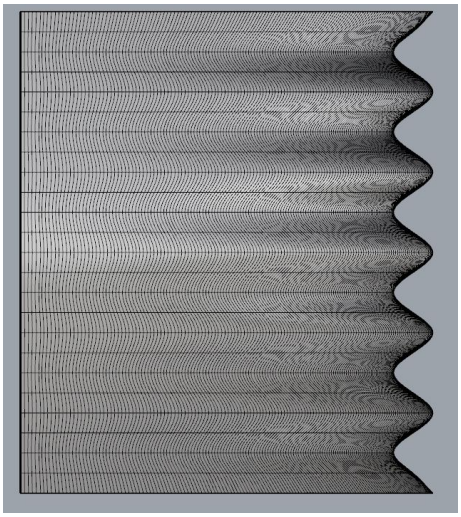

Figure 10 – Sinusoidal leading edge blade (left) and grid for numerical computations (right)

Numerical performance prediction

Flow inside the modified impeller was then simulated with the same approach of the datum impeller; performance of both are compared in Table 4. The modified impeller has an 8% increase in pressure rise capability and a 7% decrease in power.

Table 4 – Comparison of measured and computed pressure rise and power for datum and modified impellers for Q=0.26 m^3/s

	Δp_{stat}	Power
Datum impeller	203 Pa	69.6 W
Modified impeller	220 Pa	64.6 W
Δ	+ 8 %	- 7 %

Flow survey

To understand the change in performance of the two blade geometries we investigated how the flow field was affected by the leading edge modification. In Figure 11 streamlines in the blade to blade passage are shown. Near the shroud (10 %) and at midspan (50 %) the streamlines are well aligned to the blade like in the datum impeller (Figure 6), near the backshroud (90 %) the flow is still separated, but there is an evident change in the extent of separation that here starts at about 50 % of the suction surface and does not close the entire blade-to-blade passage as in the datum impeller.

From a designer point of view it is of interest to understand how the β_1 and β_2 velocity angles are affected, Figure 12. Along a line near the leading and trailing edges (positions 1 and 2 in the insert, solid lines) the flow is strongly affected by the sinusoidal geometries, resulting in distortions of the angles that follow the patterns of the leading edge waves.

In particular, the lower 40 % of the blade is affected by a strong distortion of the working angles, that reflects the flow separation seen in Figure 11. It is an apparent worsening of the flow conditioning with respect to the datum impeller. However if we look at the profiles averaged along the blade-to-blade direction (dashed lines) there is a totally different picture: in fact the trend is linear for both β_1 and β_2, resulting in a better alignment of the flow with the leading edge of the blade and a more even distribution of work along the blade span, explaining the increase of performance of the modified impeller.

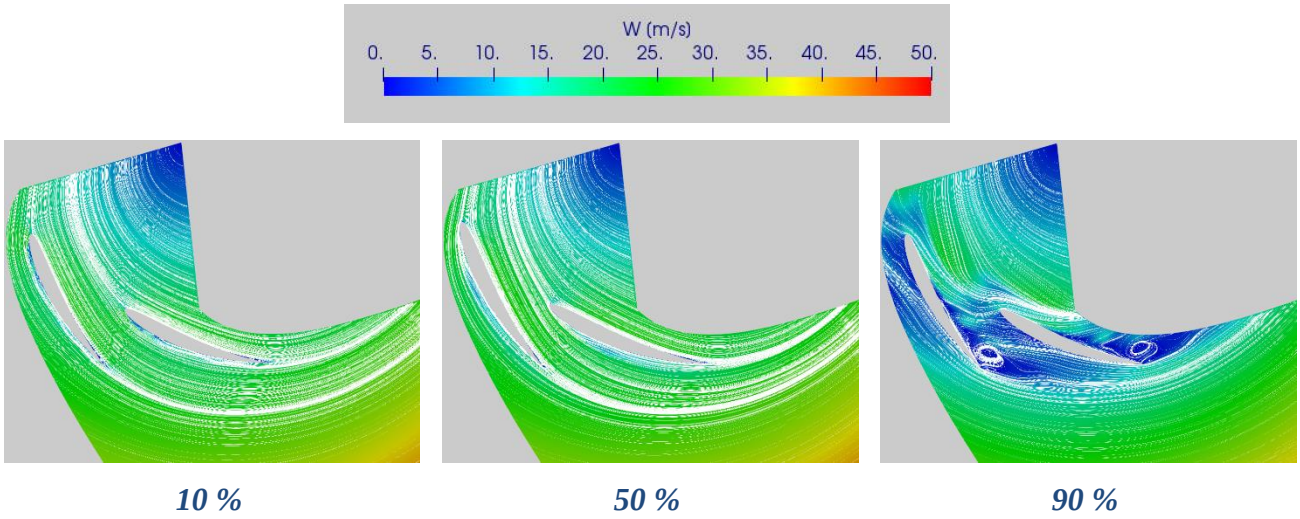

Figure 11 – Modified impeller: relative velocity streamlines over relative velocity contours for axial cross-sections at 10 % (shroud), 50 % and 90 % (back-shroud) of the blade span

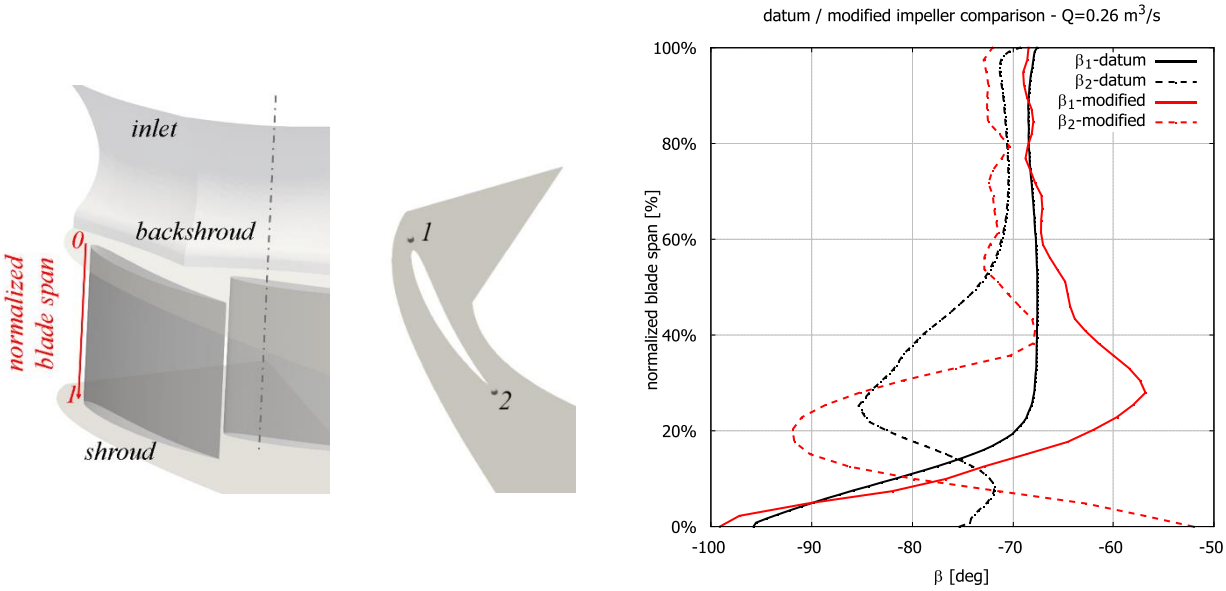

Figure 12 – Modified impeller: β_1 and β_2 spanwise distributions near the leading and trailing edges (see insert) and blade-to-blade averaged distributions (dashed lines)

Distributions of axial and radial velocity components, Figure 13, clearly show similar trends, where the most interesting part comes from the analysis of the axial velocity near the leading edge of the blade. The flow in fact is affected by the waves and even if very close to the blade there is a clear reduction of the average and peak C_{ax1} values with respect to the datum impeller, resulting in a more even inflow. This trend is confirmed also for tangential velocity components, Figure 14.

Comparison of kinematics of datum and modified impellers

In Figure 15 blade-to-blade averaged spanwise distributions of β and δ are shown in the S1 and S2 control sections. At S1 the main difference is in a lower value of β_1 for the modified impeller in the portion between 20 % and 60 % of the span, while at S2 in the same region a more complex trend is found, due to the influence of the leading edge bumps. Overall this reflects into a higher deflection capability of the modified impeller.

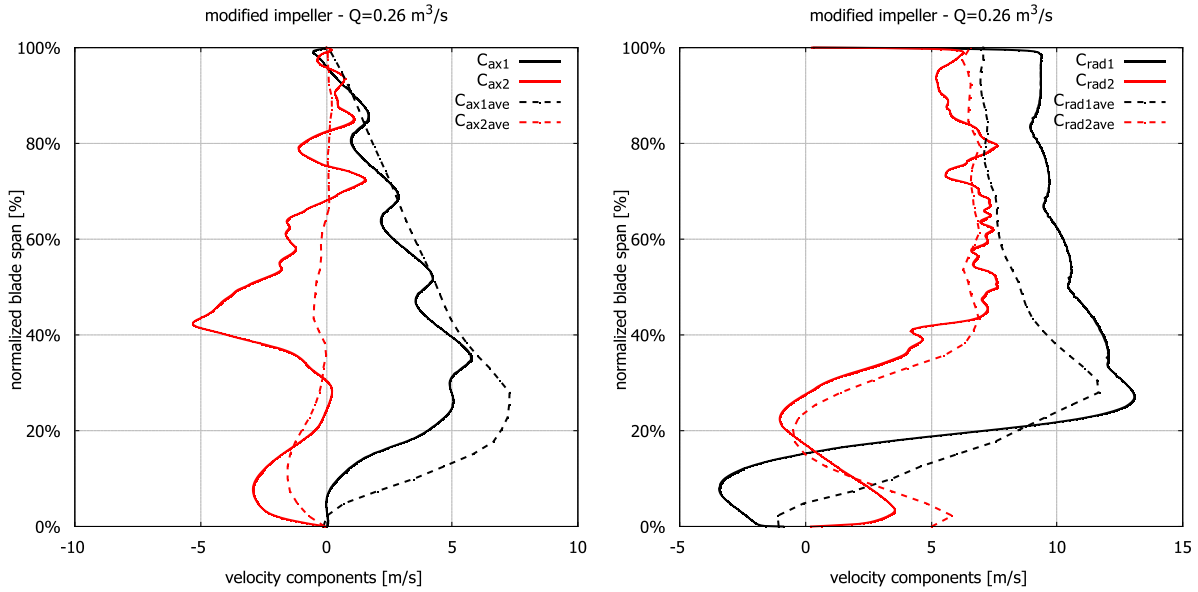

Figure 13 – Modified impeller: axial (left) and radial (right) velocity components spanwise distributions near the leading and trailing edges and blade-to-blade averaged distributions (dashed lines)

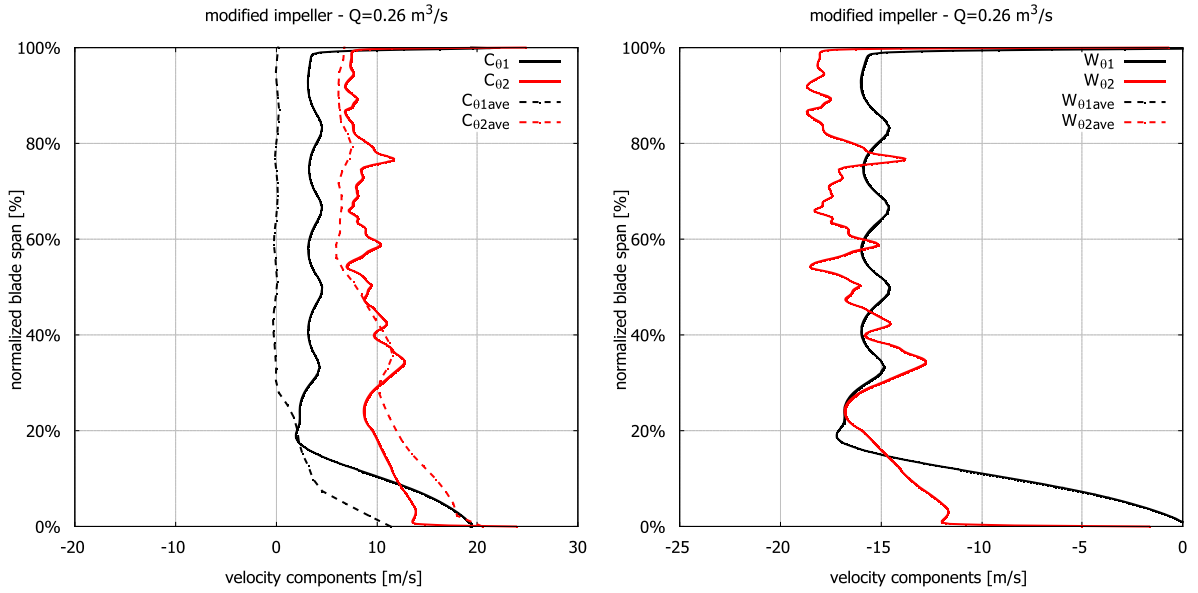

Figure 14 – Modified impeller: absolute (left) and relative (right) velocity components spanwise distributions near the leading and trailing edges and blade-to-blade averaged distributions (dashed lines)

In Figure 16 and Figure 17 blade-to-blade averaged spanwise distributions of different velocity components are shown in the same aforementioned sections. The distribution of axial and radial velocity components the fact that both impellers have similar inflow kinematics with respect to radial and axial components, as the flow rate is the same and in both cases secondary motions in axial direction are a consequence of the inflow geometry. However, due to the presence of the bumps, the tangential component is lower in the modified impeller, Figure 17. In general this trend of tangential component is true also at the impeller discharge.

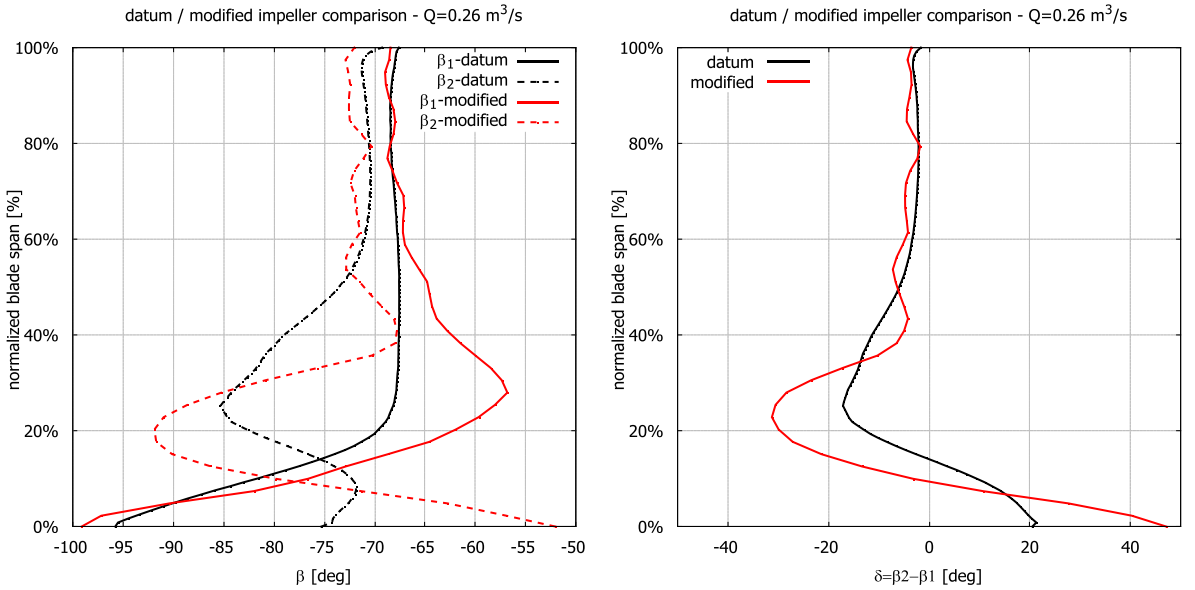

Figure 15 – Datum (black) and modified (red) impellers. β (left) and δ (right). Quantities are averaged along blade-to-blade direction.

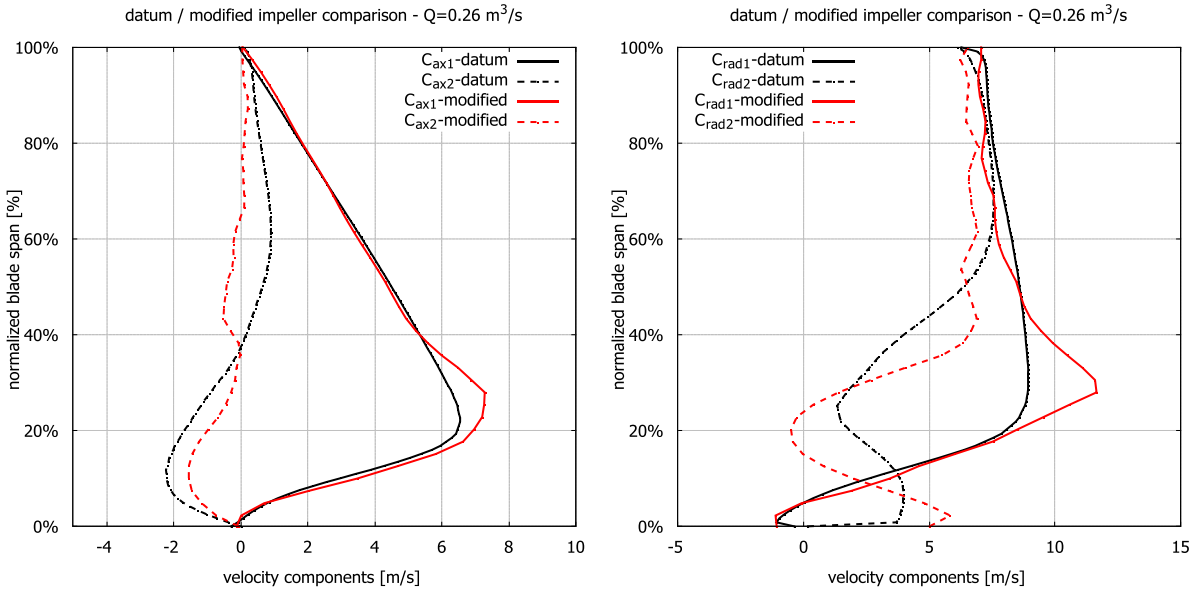

Figure 16 – Datum (black) and modified (red) impellers. Axial (left) and radial (right) velocities. Quantities are averaged along blade-to-blade direction.

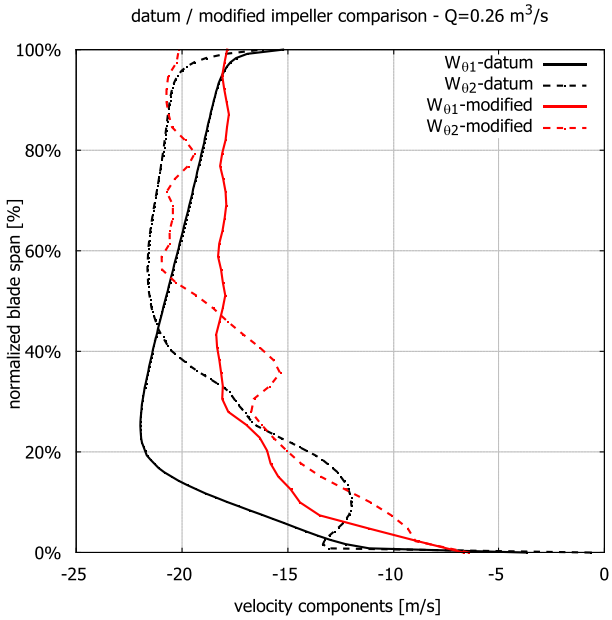

Figure 17 – Datum (black) and modified (red) impellers.
Relative tangential velocity averaged along blade-to-blade direction.

Comparison of flow fields of datum and modified impellers

In Figure 18 isocontours of helicity along the pressure and suction side of the impellers. These contours confirm the findings of [1], as the modified leading edge has a major role on the suction surface and only minor changes are found in the suction surface. In fact we can see that on the pressure side of the datum impeller a structure develops as horseshoe vortex near the leading edge and extends up to midspan in the trailing edge. The same structure is present in the modified impeller.

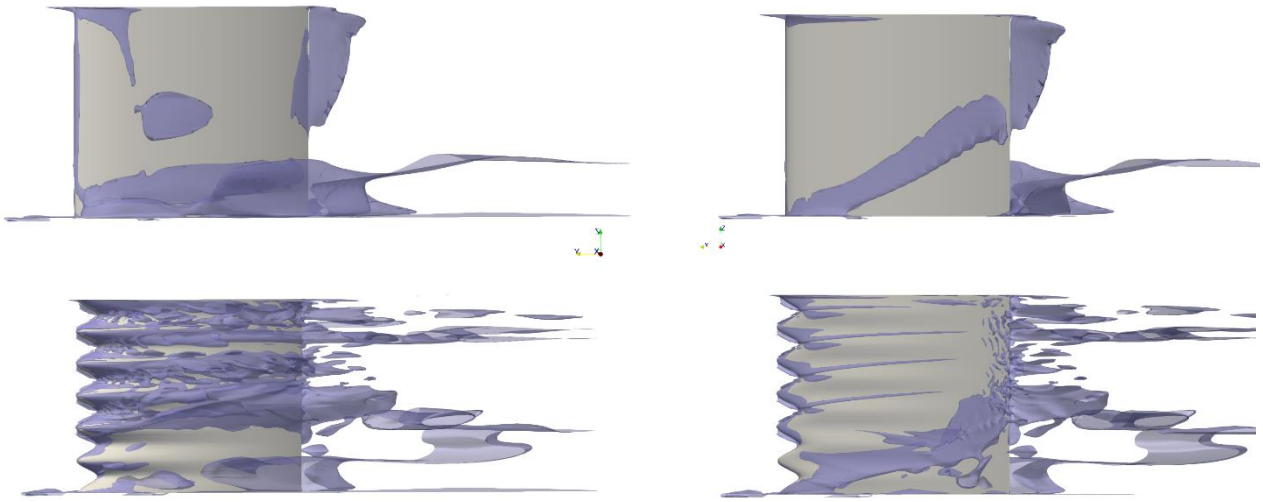

Figure 18 – Helicity contours (H=20,000) for the datum (top) and modified (bottom) impellers.
Left: suction side, right: pressure side

On the suction surface the other half of the horseshoe vortex is recognizable for the datum impeller, while a more complex series of structures is convected downstream of the wavy leading edge that are responsible for the axial redistribution of the flow.

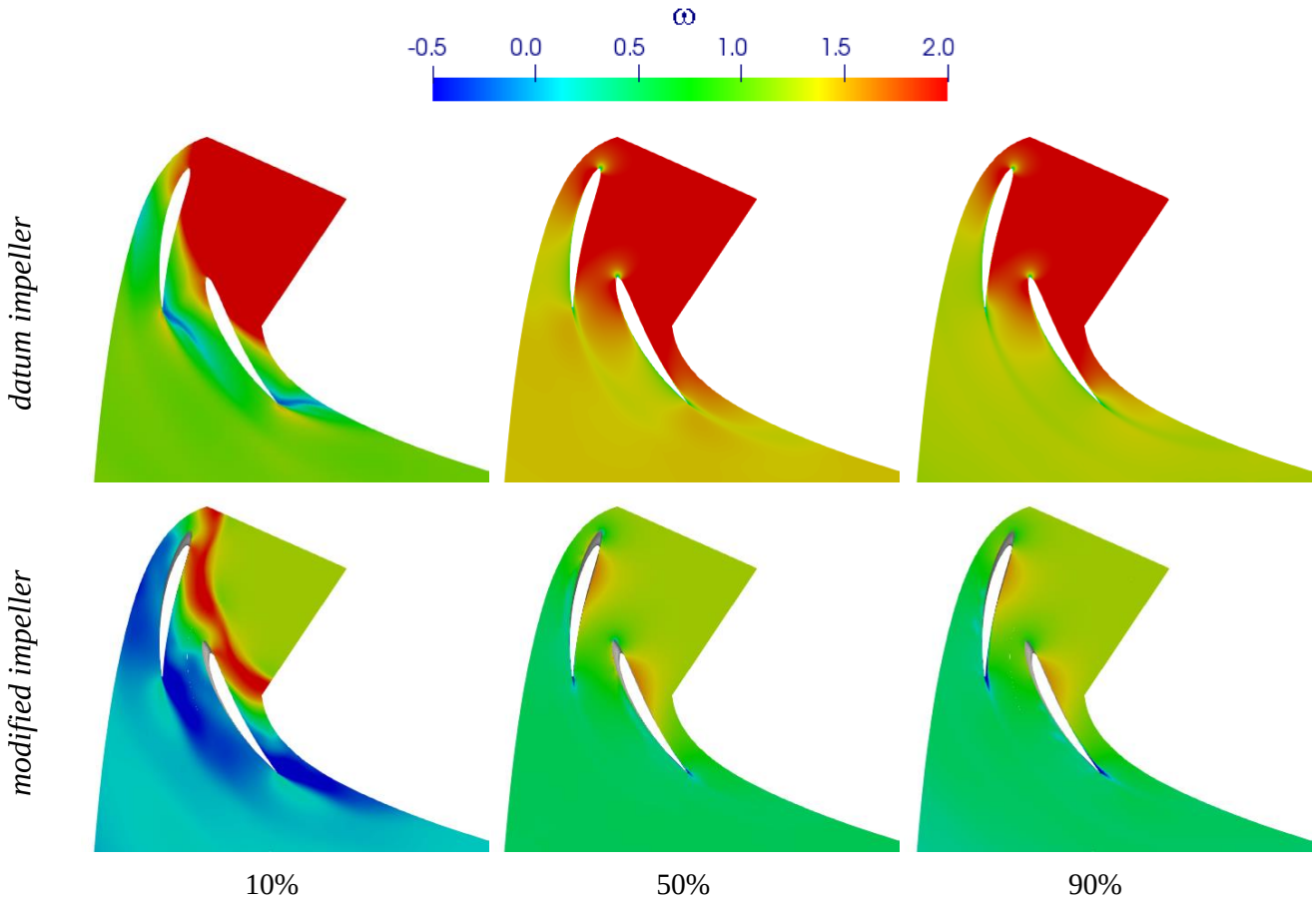

Figure 19 – Losses contours for the datum (top) and modified (bottom) impellers. Left: 10% axial span, center: midspan, right: 90% axial span

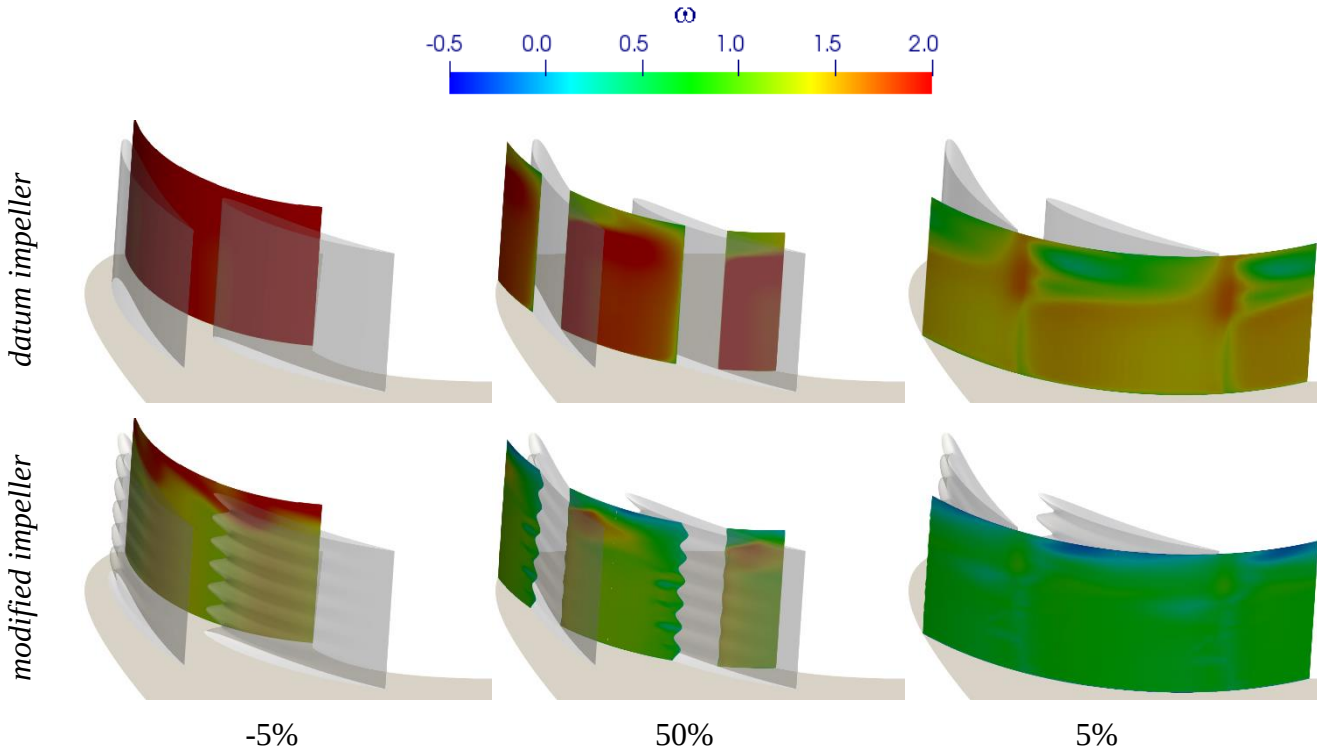

Figure 20 – Losses contours for the datum (top) and modified (bottom) impellers. Left: 10% axial span, center: midspan, right: 90% axial span

In Figure 19 and Figure 20 pressure losses, here defined as $\omega = p^*_{tot} - p_{tot} / p^*_{dyn}$ (where * refers to a quantity calculated at the throat section of the bellmouth) are plotted on three axial immersions and

three radial surfaces. From Figure 19 the major difference is in the inflow section that leads to a decrease of losses on the pressure surface up to mid-chord of the modified impeller. The same effect is evident from the evolution in radial direction shown in Figure 20, from which is evident that at the trailing edge of the blade losses are equally distributed along the span and well mixed with the modified impeller.

Off-design behavior of modified impeller

A final remark on off-duty effectiveness of the modified impeller in off-design conditions come from Table 5 and Figure 21. At higher flow rate in fact the modified impeller has again a higher pressure rise capability with lower power demands, even if the gain in both cases is reduced with respect to maximum efficiency point. Again the modified impeller show a higher deflection capability with respect to the datum impeller.

Table 5 – Comparison of measured and computed pressure rise and power for datum and modified impellers for Q=0.33 m^3/s

	Δp_{stat}	Power
Datum impeller	191 Pa	68.8 W
Modified impeller	200 Pa	67.2 W
Δ	4.7%	-2.3%

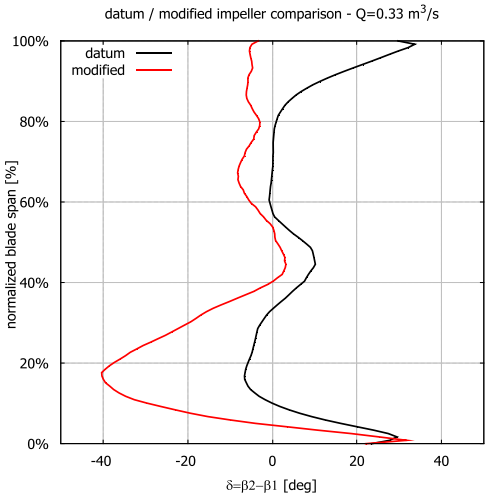

Figure 21 – Blade to blade averaged deflection δ for datum (black) and modified (red) impellers

CONCLUSIONS

The centrifugal impeller of a roof unit for civil ventilation was modified applying a sinusoidal leading edge to the rotor to control the boundary layer development along the blade. Air performance for the modified impeller lead to higher pressure rise and lower power at the duty flow rate. An analysis of the flow lead to the conclusion that the performance was related to the decrease of losses at the inflow with the modified impeller as well as to a more even distribution of velocity at the impeller exit with the sinusoidal leading edge.

BIBLIOGRAPHY

[1] A. Corsini, G. Delibra, A. G. Sheard – *The application of sinusoidal blade-leading edges in a fan-design methodology to improve stall resistance*. Proceedings of the Institution of Mechanical Engineers, Part A: Journal of Power and Energy May 2014 vol. 228 no. 3 255-271, 10.1177/0957650913514229, **2014**.

[2] Lien, F.S. & Leschziner, M.A. – *Assessment of Turbulence-transport Models Including Non-linear RNG Eddy-viscosity Formulation and Second-moment Closure for Flow over a Backward-facing Step*, Computers & Fluids vol. 23, pp. 983-1004, **1994**.

[3] AMCA 210-07 – *Laboratory Methods of Testing Fans for Certified Aerodynamic Performance Rating*. AMCA **2007**.